

Mean field initialization of the Annealed Importance Sampling algorithm for an efficient evaluation of the Partition Function of Restricted Boltzmann Machines

A. Prat Pou^a, E. Romero^b, J. Martí^a, F. Mazzanti^a

^a *Departament de Física, Universitat Politècnica de Catalunya, Barcelona Tech, Campus Nord B4-B5, E-08034, Barcelona, Spain*

^b *Departament de Ciències de la Computació, Universitat Politècnica de Catalunya, Barcelona Tech, Campus Nord B4-B5, E-08034, Barcelona, Spain*

Probabilistic models in physics often require from the evaluation of normalized Boltzmann factors, which in turn implies the computation of the partition function Z . Getting the exact value of Z , though, becomes a forbiddingly expensive task as the system size increases. This problem is also present in probabilistic learning models such as the Restricted Boltzmann Machine (RBM), where the situation is even worse as the exact learning rules implies the computation of Z at each iteration. A possible way to tackle this problem is to use the Annealed Importance Sampling (AIS) algorithm, which provides a tool to stochastically estimate the partition function of the system. So far, the standard application of the AIS algorithm starts from the uniform probability distribution and uses a large number of Monte Carlo steps to obtain reliable estimations of Z following an annealing process. In this work we show that both the quality of the estimation and the cost of the computation can be significantly improved by using a properly selected mean-field starting probability distribution. We perform a systematic analysis of AIS in both small- and large-sized problems, and compare the results to exact values in problems where these are known. As a result of our systematic analysis, we propose two successful strategies that work well in all the problems analyzed. We conclude that these are good starting points to estimate the partition function with AIS with a relatively low computational cost.

PACS numbers:

I. INTRODUCTION

The evaluation of thermodynamic potentials such as the entropy or free energy is key to understand the equilibrium properties of physical systems [1]. In real-sized classical problems, computer simulations based on Molecular Dynamics or Monte Carlo methods can not generically access them mainly because of the size of the spaces of states to sample, which grows exponentially with the number of particles. This effect is particularly easy to quantify in magnetic models of classical two-state spin systems, where the volume of the phase space grows as 2^N with N the total number of spins. Quantities such as the Helmholtz free energy F in the canonical ensemble, proportional to the logarithm of the partition function [2, 3]

$$Z = \sum_{\mathbf{x}} e^{-E(\mathbf{x})/k_B T}, \quad (1)$$

are out of reach as the sum extends over all possible states \mathbf{x} , with $E(\mathbf{x})$ the corresponding energy, k_B the Boltzmann's constant, and T the temperature. Actually, finding the value of Z is known to be an NP-hard problem [4] that therefore prevents an exact estimation unless the system is small. This same quantity, with the same problems, appears also in other areas of science, as for instance in machine learning models based on Restricted Boltzmann Machines [5, 6]. In that case the situation is even worse because Z , which is the normalization factor of a Gibbs probability distribution, has to be evaluated at each iteration in a learning scheme if the gradients of

the cost function are to be estimated exactly.

The relevance but unfortunate computational complexity implied in the determination of Z has raised the urge to devise methods to approximate it in a tractable way. One remarkable technique designed to tackle this problem was developed by Bennett [7], where the free energy difference between two overlapping canonical ensemble is estimated directly in a Monte Carlo simulation. In case one of the two values of F is known, the method allows obtain the value of the other, thus gaining access to $F = -k_B T \log(Z)$. Another interesting approach towards the evaluation of the partition function is derived from the Wang-Landau algorithm [8–10], where a stochastic exploration of the phase space is used to recover the density of energy states $\rho(E)$ corresponding to the Hamiltonian of the system under study. In this framework, the partition function is recovered as the integral of $\rho(E)e^{-E/k_B T}$ over the energy range spanned by the system configurations. This method has proved to reliably reproduce the physics of different systems as the 2D-Ising model, although it can be difficult to apply to more complex situations involving an intricated $\rho(E)$.

An alternative approach to the problem was devised in 2001 by R. M. Neal [11, 12], the Annealed Importance Sampling algorithm, where an annealing procedure is implemented to obtain reliable samples from an otherwise intractable probability distribution starting from samples of a simpler and tractable one. In this method, the partition function is one of the simplest quantities to evaluate, although as in most sampling schemes, convergence towards the exact value of Z is only guaranteed in the in-

finite limit, both in number of samples and intermediate annealing steps. In practical terms, when a finite number of samples and intermediate annealing chains is employed, the predicted value of Z depends on the different simulation inputs, particularly on the initial probability distribution.

Surprisingly, and despite its broad formulation in terms of an initial and a final probability distributions, little use has been seen of the AIS algorithm in the numerical simulation of physical systems to the best of our knowledge. More application has emerged in the world of neural networks, particularly in the field of RBMs [5], where the evaluation of Z is key to a precise optimization of the system parameters along learning. In this context, the AIS algorithm turns out to be most efficient since the random walk exploration can be performed by means of Gibbs sampling, which is fully parallelizable [13]. Finally, the AIS algorithm is particularly suited to address binary state unit problems like spin systems or RBMs where the different probability distributions involved along the annealing chains are cost-effective and simple to evaluate.

In this work we study how AIS can be used to produce reliable estimates of $\log(Z)$ in RBMs and systems that can be mapped to them. Our goal is to achieve that with a small computational cost, even in realistically large problems, when a suitable starting probability distribution is employed. We discuss how to obtain the optimal mean field probability distribution $p_0^*(\mathbf{x})$ that is closest to the Boltzmann distribution of the real model under study. After a brief derivation of how to get $p_0^*(\mathbf{x})$ from average system properties, we propose two strategies to find approximations to it in both artificial sets and magnetic spin systems where the exact value of the partition function can be determined. Finally, we compare the results obtained with the standard procedure, where the uniform probability distribution is employed as the starting point of the AIS algorithm.

II. ANNEALED IMPORTANCE SAMPLING

The AIS algorithm, developed by R. Neal in the late 90's [11, 12] allows sampling from a probability distribution that would otherwise be intractable. It can be used to estimate Z , but it is more general and allows finding approximate values of any observable quantity $\alpha(\mathbf{x})$ over a probability distribution $p(\mathbf{x})$. In a general sense, this computation can be very inefficient due to two main reasons. On one hand, the probability distribution $p(\mathbf{x})$ can be impossible to sample because the exact form of $p(\mathbf{x})$ is not known, as it happens in many quantum physics problems [14–16]. On the other hand, the number of samples required to obtain an accurate estimate of the average value of $\alpha(\mathbf{x})$ may be unreasonably large. In order to deal with these problems, one usually resorts to some form of Importance Sampling, where the exploration of the space is guided by a known and suitable probability

distribution $q(\mathbf{x})$ [17]. In this way one typically evaluates

$$\langle \alpha \rangle = \int d\mathbf{x} q(\mathbf{x}) \left(\frac{p(\mathbf{x})\alpha(\mathbf{x})}{q(\mathbf{x})} \right). \quad (2)$$

using stochastic techniques, where samples are drawn from $q(\mathbf{x})$. Importance Sampling is employed to reduce the variance of the estimator, or to reduce the number of samplings needed to achieve the same statistical accuracy. In any case, Importance Sampling can only be performed when a suitable $q(\mathbf{x})$ is at hand, but that may not always be the case. The AIS method allows building $q(\mathbf{x})$ starting from a trivial probability distribution, and performing an annealing process through a set of intermediate distribution corresponding to decreasing temperatures.

As explained in [11, 12], in order to estimate $\langle \alpha \rangle$ starting from a trivial $p_0(\mathbf{x})$, one builds a chain of intermediate distributions $p_i(\mathbf{x})$ that interpolate between $p_0(\mathbf{x})$ and $p_n(\mathbf{x}) = p(\mathbf{x})$. Denoting by $\tilde{p}_k(\mathbf{x}) = Z_k p_k(\mathbf{x})$ the corresponding unnormalized probability distributions, a common scheme is to define

$$\tilde{p}_k(\mathbf{x}) = \tilde{p}_0(\mathbf{x})^{1-\beta_k} \tilde{p}_n(\mathbf{x})^{\beta_k}, \quad (3)$$

with $0 = \beta_0 < \beta_1 < \dots < \beta_n = 1$ and $N_\beta = n + 1$. The approach used in AIS is to turn the estimation of $\langle \alpha \rangle$ into a multidimensional integration of the form

$$\langle \alpha \rangle = \int d\mathbf{x}_1 \dots d\mathbf{x}_n g(\mathbf{x}_1, \dots, \mathbf{x}_n) \frac{f(\mathbf{x}_1, \dots, \mathbf{x}_n)}{g(\mathbf{x}_1, \dots, \mathbf{x}_n)} \alpha(\mathbf{x}_n), \quad (4)$$

where

$$f(\mathbf{x}_1, \dots, \mathbf{x}_n) = p_n(\mathbf{x}_n) \prod_{j=1}^{n-1} \hat{T}_j(\mathbf{x}_{j+1}, \mathbf{x}_j) \quad (5)$$

$$g(\mathbf{x}_1, \dots, \mathbf{x}_n) = p_0(\mathbf{x}_1) \prod_{j=1}^{n-1} T_j(\mathbf{x}_j, \mathbf{x}_{j+1}) \quad (6)$$

are normalized joint probability distributions for the set of variables $\{\mathbf{x}_1, \dots, \mathbf{x}_n\}$. In these expressions $T_k(\mathbf{x}, \mathbf{y})$ represents a transition probability of moving from state \mathbf{x} to state \mathbf{y} , which asymptotically leads to the equilibrium probability $p_k(\mathbf{x})$. In the same way, $\hat{T}_k(\mathbf{y}, \mathbf{x})$ represents the reversal of $T_k(\mathbf{x}, \mathbf{y})$. The detailed balance condition implies that the transition probabilities fulfill the relation

$$\hat{T}_j(\mathbf{y}, \mathbf{x}) = T_j(\mathbf{x}, \mathbf{y}) \frac{p_j(\mathbf{x})}{p_j(\mathbf{y})} \quad (7)$$

in order to be able to sample the space ergodically [18]. Therefore, $\langle \alpha \rangle$ can be estimated from Eq. (4) with

$$\frac{f(\mathbf{x}_1, \dots, \mathbf{x}_n)}{g(\mathbf{x}_1, \dots, \mathbf{x}_n)} = \prod_{k=1}^n \frac{p_k(\mathbf{x}_k)}{p_{k-1}(\mathbf{x}_k)}, \quad (8)$$

as $g(\mathbf{x}_1, \dots, \mathbf{x}_n)$ is easily sampled from the trivial $p_0(\mathbf{x})$.

In practice, one uses $g(\mathbf{x}_1, \dots, \mathbf{x}_n)$ to generate N_s samples of all the intermediate distributions, such that for every set of values $\{\mathbf{x}_1^i, \mathbf{x}_2^i, \dots, \mathbf{x}_n^i\}$, with $i = 1, 2, \dots, N_s$, one gets a set of weights $\{\omega_i\}$ upon substitution in Eq. (8). In this way, $\langle \alpha \rangle$ is estimated according to

$$\langle \alpha \rangle \approx \frac{\sum_{i=1}^{N_s} \omega_i \alpha(\mathbf{x}_n^i)}{\sum_{i=1}^{N_s} \omega_i}, \quad (9)$$

with

$$\omega_i = \prod_{k=1}^n \frac{p_k(\mathbf{x}_k^i)}{p_{k-1}(\mathbf{x}_k^i)} = \frac{Z_0}{Z_n} \prod_{k=1}^n \frac{\tilde{p}_k(\mathbf{x}_k^i)}{\tilde{p}_{k-1}(\mathbf{x}_k^i)} = \frac{Z_0}{Z_n} \tilde{\omega}_i, \quad (10)$$

which defines the set of importance weights $\{\tilde{\omega}_i\}$ obtained from the product of the ratios of the unnormalized probabilities. Notice that $\tilde{\omega}_i$ is an accessible quantity, while ω_i is not, just because one does not have access to Z_n . One important consequence of this formalism is that a simple estimator of the partition function Z_n associated to the distribution $p_n(\mathbf{x}) = p(\mathbf{x})$ is directly given by the average value

$$\frac{Z_n}{Z_0} \approx \frac{1}{N_s} \sum_i \tilde{\omega}_i. \quad (11)$$

Since the values of $\tilde{\omega}_i$ are usually large, one typically draws samples of $\log(\tilde{\omega}_i)$. In this way, one uses a set of Z_0 -normalized AIS samples $s_i = \log(\tilde{\omega}_i) + \log(Z_0)$, such that

$$\log(Z_n) \approx \log \left[\frac{1}{N_s} \sum_i e^{s_i} \right] = \log(Z_{\text{AIS}}), \quad (12)$$

and defines Z_{AIS} as an approximation to Z_n . Notice that this value is different from the mean of the samples s_i , although these two quantities do not differ much when the variance of the samples is small. In fact, these two quantities tend to be the same when the variance of the set of samples is small compared to the mean value. In other situations, the nonlinear character of the operation in Eq. (12) makes the result be dominated by the largest samples, to the point that, in the extreme case, the largest sample exhausts the total sum.

III. THE RESTRICTED BOLTZMANN MACHINE

A RBM with binary units is a spin model describing a mixture of two different species, where intra-species interactions are forbidden, and units play the role of the spins. In general, though, RBM units take $[0, 1]$ values rather than $[-1, 1]$. Furthermore, only one component of this mixture is assumed to be accessible to the external observer, usually called the *visible layer*. The other species, usually called *hidden layer*, is assumed to have no contact with the outside world, and is present to build

up correlations in the model. As a consequence, one is only interested in the marginal probability distribution associated to the visible units.

The energy function of a binary RBM with N_v visible units \mathbf{x} and N_h hidden units \mathbf{h} , is defined as [19, 20]:

$$E(\mathbf{x}, \mathbf{h}) = -\mathbf{x}^T \mathbf{b} - \mathbf{c}^T \mathbf{h} - \mathbf{x}^T \mathbf{W} \mathbf{h}, \quad (13)$$

where \mathbf{W} is the two-body weights matrix setting the coupling strength between the two species, while \mathbf{b} and \mathbf{c} represent the external fields acting on each layer and are generically denoted as *bias*. In this expression, \mathbf{x}^T stands for the transpose of vector \mathbf{x} .

The energy in Eq. (13) can be cast as a quadratic form, where visible and hidden units are organized as row and column vectors preceded by a constant value of 1 to account for the bias terms

$$\tilde{\mathbf{x}}^T = (1 \ x_1 \ x_2 \ \dots \ x_{N_v}) \quad , \quad \tilde{\mathbf{h}}^T = (1 \ h_1 \ h_2 \ \dots \ h_{N_h}) \quad , \quad (14)$$

leading to

$$E(\tilde{\mathbf{x}}, \tilde{\mathbf{h}}) = -\tilde{\mathbf{x}}^T \begin{pmatrix} 0 & \mathbf{c}^T \\ \mathbf{b} & \mathbf{W} \end{pmatrix} \tilde{\mathbf{h}} \equiv -\tilde{\mathbf{x}}^T \tilde{\mathbf{W}} \tilde{\mathbf{h}}, \quad (15)$$

where $\tilde{\mathbf{W}}$ is the *extended* weights matrix, which includes the bias terms.

As usual in energy-based models, the probability of a state (\mathbf{x}, \mathbf{h}) follows a Boltzmann distribution

$$p(\mathbf{x}, \mathbf{h}) = \frac{e^{-E(\mathbf{x}, \mathbf{h})/T}}{Z}, \quad (16)$$

with

$$Z = \sum_{\mathbf{x}, \mathbf{h}} e^{-E(\mathbf{x}, \mathbf{h})/T} \quad (17)$$

and k_B set to 1. The particular form of the energy function (13) makes both $P(\mathbf{h}|\mathbf{x})$ and $P(\mathbf{x}|\mathbf{h})$ to factorize as a product of probabilities corresponding to independent random variables. As a consequence, Gibbs sampling can be efficiently used to compute them [21]. In addition, it is also possible to evaluate one of the two sums involved in the partition function. In this way, for $[0, 1]$ units, one has

$$Z = \sum_{\mathbf{x}} e^{\mathbf{x}^T \mathbf{b}/T} \prod_j \left(1 + e^{(\mathbf{c}_j + \mathbf{x}^T \mathbf{w}_j)/T} \right), \quad (18)$$

where index j runs over the whole set of hidden units, and \mathbf{w}_j stands for the j th column of \mathbf{W} . However, the evaluation of Z is still prohibitive when the number of input and hidden variables is large, since it involves an exponentially large number of terms. For that reason, RBMs are computationally hard to evaluate or simulate accurately [22].

IV. DATASETS

In this work we explore different problems where $\log(Z)$ can be exactly computed, which will be then used to benchmark the approximations described afterwards. At the end, these are employed to predict the value of $\log(Z)$ on a large, realistic system where an exact evaluation is prohibitive. The set of models where the exact $\log(Z)$ is accessible include artificially generated weights, RBM learning weights, and magnetic spin systems that can be directly mapped into an RBM. These include:

- 1) Gaussian Weights with Gaussian Moments (GWGM), characterized by an extended matrix of weights $\tilde{\mathbf{W}}$ of Gaussian random numbers with $N_v = 20$ and $N_h = 180$. The mean value and the standard deviation of each set of weights are also sampled from a Gaussian distribution with $\mu = -10, \sigma = 10$, and $\mu = 20, \sigma = 10$, respectively. The temperature for all these models has been set to 1. Due to the reduced value of N_v , the exact calculation of Z can be performed by brute force, and we have generated a total of 100 models.
- 2) A set of weights obtained after training a RBM with the MNIST dataset [23], with $N_h = 20$ hidden units (MNIST-20h), similar to the simple case studied in Ref. [13] We monitor and store the weights along the learning process with the aim of having a complete picture of their evolution. In this way, we have snapshots taken at the beginning of the learning, where the training set typically does not correspond to the highest probability states, and at the end, where they are supposed to carry most of the probability mass. As in the GWGM dataset, T is set to 1.

These two datasets use $[0, 1]$ binary visible and hidden variables.

- 3) Classical Ising and Spin Glass models in one and two dimensions. A one-dimensional Ising model with periodic boundary conditions containing an even number of spins $\{s_1, s_2, \dots, s_{2N}\}$ can be represented by a RBM with the same number of units in each layer. Identifying even and odd spins with hidden and visible units, respectively, one has

$$\begin{aligned} \mathbf{b}^T &= (B_1, B_3, \dots, B_{2N-1}) \\ \mathbf{c}^T &= (B_2, B_4, \dots, B_{2N}) \end{aligned}$$

and

$$\mathbf{W} = \begin{pmatrix} J_{1,2} & 0 & 0 & \cdots & J_{N,1} \\ J_{2,3} & J_{3,4} & 0 & \cdots & 0 \\ 0 & J_{4,5} & J_{5,6} & \cdots & 0 \\ \vdots & \vdots & \vdots & \ddots & \vdots \\ 0 & 0 & 0 & \cdots & J_{N-1,N} \end{pmatrix},$$

where $J_{i,i+1}$ is the interaction between spins s_i and s_{i+1} . Only two entries per row/column can be non-zero in this arrangement. In the Ising model (1DIsing), $J_{i,i+1} = J$ and $B_i = B$ for all spins, while they can take different values in what we denote as a Spin Glass model (1DSG). The partition function of 1DIsing and 1DSpinGlass can be easily computed using the Transfer Matrix formalism [24, 25]. We have generated 3 sets of 100 1DIsing models, as well as 3 sets of 100 1DSG models, all of them containing $N_s = 200$ spins. In both cases (Ising and Spin Glass) the $J_{i,j}$ and B_i Hamiltonian parameters have been drawn at random from a Normal distribution with $\mu = -100$ and $\sigma = 200$, for three different temperatures $T = 10$ (1DIsing1 and 1DSG1), $T = 1$ (1DIsing2 and 1DSG2), and $T = 0.1$ (1DIsing3 and 1DSG3).

The two-dimensional square-lattice Ising model is much harder to solve and its analytic solution was given by Onsager in [26] in the absence of an external field. Similar to the 1D models, it can be represented by an RBM, where visible and hidden units are arranged in a checkerboard configuration. In this case, four weights can be non-zero in each row and column of $\tilde{\mathbf{W}}$ since there are no bias terms. Three sets of 100 2DIsing models (2DIsing1, 2DIsing2 and 2DIsing3) corresponding to $N_s = 256$ spins have been generated, with parameters drawn from the same normal distributions used for the previous 1D cases, and the same temperatures.

Furthermore, we have extend that to what we name a 2D Spin Glass (2DSG), where all two-body $J_{i,j}$ correlations are different, while keeping the connectivity restricted to nearest neighbors. In this case the partition function is computed by *brute force*, which limits the size of the square lattices to be less than or equal to 6×6 , as an even number of spins per dimension is required in order to properly satisfy the periodic boundary conditions. Two different sets of 50 models (2DSG1 and 2DSG2) have been used, drawn from a normal distribution with $\mu = 10^4$ and $\sigma = 10^4$ and corresponding to $T = 10$ and $T = 0.1$, respectively.

All these models use $[-1, 1]$ spin variables as standard.

Finally, we also analyze the MNIST dataset with a RBM containing $N_h = 500$ hidden units (MNIST-500h), where no exact value of $\log(Z)$ is known. As in the MNIST-20h, they are the result of a learning process with $T = 1$ and $[0, 1]$ units.

V. THE OPTIMAL MEAN FIELD APPROXIMATION

The equilibrium Boltzmann distribution associated to any physical system is given by

$$p(\mathbf{x}) = \frac{e^{-E(\mathbf{x})/T}}{Z}, \quad (19)$$

where $E(\mathbf{x})$ is the system's energy corresponding to state \mathbf{x} . In the spirit of AIS, the partition function associated to $p_n(\mathbf{x})$ can be obtained from a chain of intermediate probability distributions that start from another, much simpler and easy to sample $p_0(\mathbf{x})$, as shown in Sec. II. Getting a good $p_0(\mathbf{x})$ can ease the job to AIS, and becomes therefore a key ingredient to get an accurate estimation of $\log(Z)$ with a reasonable number of intermediate chains and samples. A very simple probability distribution $p_0(\mathbf{x})$ can be obtained from a mean-field model containing only external fields \mathbf{B} . In this scheme, and for an RBM, $E_0(\mathbf{x}) = -\mathbf{x}^T \mathbf{B}$ defines the starting mean field energy, which makes

$$p_0(\mathbf{x}) = \frac{2^{N_h} e^{\mathbf{x}^T \cdot \mathbf{B}/T}}{Z_0} \quad (20)$$

be the product of independent distributions for each unit, thus allowing for a very simple and efficient sampling scheme in parallel. Furthermore, for $[0, 1]$ binary units, the corresponding partition function reads

$$Z_0 = 2^{N_h} \prod_{j=1}^{N_v} (1 + e^{B_j/T}) \quad (21)$$

while for $[-1, 1]$ units one has

$$Z_0 = 2^{N_v + N_h} \prod_{j=1}^{N_v} \cosh(B_j/T). \quad (22)$$

Despite dealing with a mean field, getting the most suitable \mathbf{B} may not be a trivial task. In most practical applications, and with lack of a better model, the simplest choice $\mathbf{B} = 0$ is adopted, thus turning $p_0(\mathbf{x})$ into the uniform probability distribution. In the spirit of the AIS algorithm, and according to the theoretical development [11, 12], one then expects that increasing the number of intermediate distributions should lead to the exact result, no matter what the starting $p_0(\mathbf{x})$ is. Whilst this should be the case, it is not clear how the dynamics of this process is, and whether the desired limit is attained with a large but manageable number of intermediate distributions. In other words, one has no clue as to what the convergence properties of the algorithm are, other than knowing that it provides the right result in the infinite limit. In order to test that in practice, we have conducted different experiments with the GWGM and MNIST-20h datasets of Sec. IV. Figure 1 shows the evolution of the prediction of $\log(Z)$ with N_β for the MNIST-20h (left

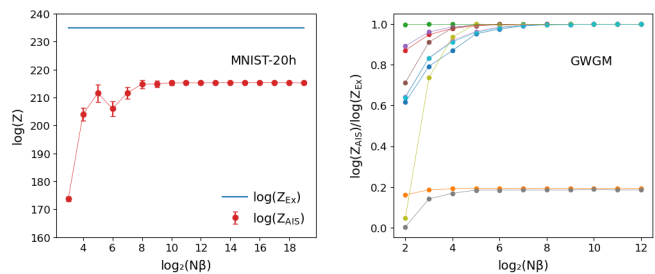


FIG. 1: AIS estimation of $\log(Z)$ starting from $\mathbf{B} = 0$ for the MNIST-20h (left) and ten different GWGM datasets (right) as a function of the number N_β of intermediate distributions. The left panel shows both the exact value (in blue) and the AIS estimations, while on the right the ratio of these two quantities is plotted.

panel) and 10 randomly selected GWGM weights (right panel). In all these calculations, a total of $N_s = 1024$ AIS samples have been employed to build $\log(Z_{AIS})$ according to Eq. (12). In the MNIST-20h, both the exact and the predicted values are displayed, while in the GWGM case the ratio of the AIS $\log(Z)$ to the exact $\log(Z)$ is displayed for the sake of clarity. The errorbars are obtained after averaging 100 repetitions of the same experiments.

Two immediate conclusions can be drawn from Fig. 1. On one hand, it is clear that in both cases a stable prediction has been achieved already at $N_\beta = N_s = 1024$. This fact has also been observed with the other datasets tested. Starting from there, we have set $N_\beta = 4096$ and $N_s = 1024$ in all the following AIS runs all over this work, which seems to be large enough to get stable results while still allowing for a fast evaluation of $\log(Z)$ with a standard computer. On the other hand, one readily notices that, despite providing an apparently converged result, the AIS prediction starting from $\mathbf{B} = 0$ may differ substantially from the exact result, even in cases where one of the dimensions of the problem (N_v or N_h) is small. The situation is even worse as the errorbars diminish with increasing N_β , leading to the false impression that a reliable prediction has been achieved. The results in the left panel show that this picture remains unaltered even with $N_\beta = 2^{20}$, thus indicating that probably a completely unpractical amount of intermediate distributions is needed to produce the required changes to bring the AIS prediction close to the exact result, something that is guaranteed in the asymptotic limit [11, 12].

Still, the plots in Fig. 1 yield a discouraging picture about the possibility of achieving good results starting from $\mathbf{B} = 0$, an image that should be properly put into perspective. In order to get a more complete view we have conducted AIS experiments starting from $\mathbf{B} = 0$ on all the datasets of Section IV. We have computed 100 independent repetitions in all cases, consisting each in $N_s = 1024$ AIS samples with $N_\beta = 4096$. For every

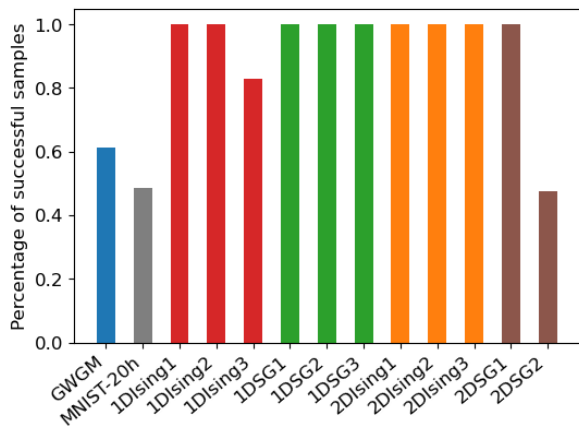


FIG. 2: Percentage of AIS samples producing an estimation of $\log(Z)$ with a relative error of less than 5% with respect to the exact result, obtained starting from $\mathbf{B} = 0$. The results have been averaged over all models of each tested dataset.

model, an estimation of $\log(Z)$ has been obtained from the 1024 samples using Eq.(12), and the relative error

$$\epsilon_r = \left| \frac{\log(Z_{\text{AIS}}) - \log(Z_{\text{Ex}})}{\log(Z_{\text{Ex}})} \right|, \quad (23)$$

has been subsequently computed and averaged over all models belonging to the same dataset. The result is shown in Fig. 2, and displays the percentage of samples fulfilling the condition $\epsilon_r \leq 0.05$. As it can be seen, the choice $\mathbf{B} = 0$ works in many cases, but not in all of them.

In any case, and despite the fact that the uniform probability distribution corresponding to $\mathbf{B} = 0$ provides a trivial starting point, it is not the only possible simple choice. In fact, any distribution of the mean field form given in Eq. (20) is suitable to start AIS from, as with that all components of \mathbf{x} become independent random variables that can be sampled in parallel. Among all the possible choices of \mathbf{B} , therefore, one can look for the optimal one that produces the best possible results with little computational cost. In this context, being optimal means to produce a mean field probability distribution that is closest to the actual $p_n(\mathbf{x})$ one seeks to sample, according to some metric.

In particular, the optimal values \mathbf{B}^* of \mathbf{B} can be obtained minimizing the Kullback-Leibler (KL) divergence between $p_0(\mathbf{x})$ and the full RBM probability distribution $p_n(\mathbf{x})$, so we impose the condition

$$\nabla_{\mathbf{B}} \sum_{\mathbf{x}} p_n(\mathbf{x}) \log \left(\frac{p_n(\mathbf{x})}{p_0(\mathbf{x})} \right) \Bigg|_{\mathbf{B}=\mathbf{B}^*} = 0,$$

where the sum over \mathbf{x} extends to all the 2^{N_v} states as hidden states have already been marginalized in both $p_0(\mathbf{x})$

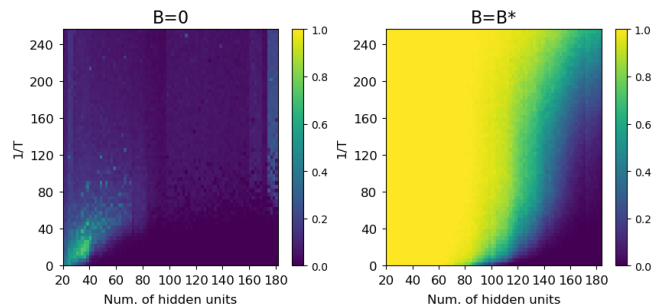


FIG. 3: Percentage of AIS samples producing a relative error lower or equal to 5% with respect to the exact $\log(Z)$ value, as a function of the number of hidden units and inverse temperature. The left and right panels show the results starting from $\mathbf{B} = 0$ and $\mathbf{B} = \mathbf{B}^*$, respectively.

and $p_n(\mathbf{x})$. One thus have, for $x_i \in [0, 1]$

$$\begin{aligned} 0 &= - \sum_{\mathbf{x}} p_n(\mathbf{x}) \nabla_{\mathbf{B}} \log p_0(\mathbf{x}) \Bigg|_{\mathbf{B}=\mathbf{B}^*} \\ &= - \frac{1}{T} \sum_{\mathbf{x}} p_n(\mathbf{x}) \mathbf{x} + \sum_{\mathbf{x}} p_n(\mathbf{x}) \nabla_{\mathbf{B}} \log Z_0 \Bigg|_{\mathbf{B}=\mathbf{B}^*} \\ &= - \langle \mathbf{x} \rangle_n + \frac{1}{1 + e^{-\mathbf{B}^*/T}}, \end{aligned} \quad (24)$$

where the subscript n indicates that the average values are taken over the $p_n(\mathbf{x})$ probability distribution corresponding to the target RBM. In this way one gets, for $x_i \in [0, 1]$

$$\mathbf{B}^* = -T \log \left(\frac{1}{\langle \mathbf{x} \rangle_n} - 1 \right) \quad (25)$$

for each visible unit $i \in \{1, 2, \dots, N_v\}$. For $x_i \in [-1, 1]$, a similar procedure leads to

$$\mathbf{B}^* = -T \tanh^{-1}(\langle \mathbf{x} \rangle_n). \quad (26)$$

These expressions imply that the problem of finding \mathbf{B}^* is equivalent to obtaining the exact average values of the visible units, which may not be a trivial task depending on the problem at hand.

In order to test the benefits of using \mathbf{B}^* , we perform several AIS runs starting from the optimal $p_0^*(\mathbf{x}) = 2^{N_h} e^{\mathbf{B}^* \cdot \mathbf{x}/T} / Z_0$ and compare the results to the same calculations starting from the uniform probability distribution, corresponding to $\mathbf{B} = 0$. As stated above, in both cases we use $N_\beta = 4096$ intermediate chains to obtain $N_s = 1024$ AIS samples. Figure 3 shows the results obtained in colormap form for one of the most difficult GWGM cases. The horizontal axis indicates the number n_h of hidden units considered, spanning the range from 1 to $N_h = 180$, obtained by discarding weights (that is, setting $\omega_{ij} = 0$ for $j > n_h$), while the vertical axis displays

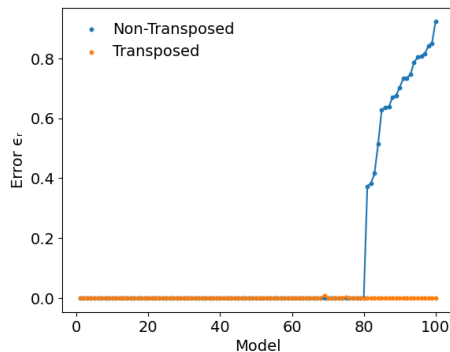


FIG. 4: Relative error of all models in the transposed and non-transposed GWGM datasets, computed as in Eq. (23). For the sake of clarity, the models have been sorted according to the relative error of the non-transposed results.

the inverse temperature. In all cases we use $N_v = 20$ visible units, as described in Sec. IV, thus allowing for the exact calculation of $\log(Z)$ by *brute force*. The maps show the percentage of the 1024 samples of $\log(Z)$ that differ from the exact value by less than 5% in each case. As it can be readily seen, the fact that $p_0^*(\mathbf{x})$ is *closer* to the RBM probability distribution makes AIS work less and perform better, as expected. Notice, though, that for some combinations of T and n_h the efficiency of AIS suffers even when starting from $p_0^*(\mathbf{x})$. This should not be completely surprising, mostly considering that a mean field starting probability distribution can still be too far away from that of the actual RBM, thus indicating that one should look for a different (and unknown) starting probability distribution.

The right panel in Fig. 3 suggests also that a mean field starting point can be problematic when the number of hidden units is much larger than the number of visible ones. This problem is easily solved noticing that $\log(Z)$ is invariant under the exchange of \mathbf{x} and \mathbf{h} in the RBM, associated to replacing the array of weights by its transpose. Based on these results, we have conducted additional tests on the whole GWGM dataset. In fact, the expectation values $\langle \mathbf{x} \rangle_n$ can always be evaluated when the dimension of the hidden space is small, as in the present case. It is easy to show that, for binary $[0, 1]$ units, one has

$$\langle \mathbf{x} \rangle_n = \sum_{\mathbf{h}} p_n(\mathbf{h}) \prod_{i=1}^{N_v} \frac{1}{1 + e^{-(b_i + \mathbf{W}^i \mathbf{h})/T}}, \quad (27)$$

where the sum extends over all hidden states, while $p_n(\mathbf{h})$ and \mathbf{W}^i stand for the hidden state probability and the i -th row of the two-body weights matrix, respectively. Figure 4 shows the relative error obtained after averaging ten repetitions of each AIS run, for the 100 GWGM models at $T = 1$. All runs started from \mathbf{B}^* computed from the

exact $\langle \mathbf{x} \rangle_n$, for the transposed and non-transposed configurations. Results have been sorted in ascending error order of the non-transposed configurations in order to get a better view. As it can be seen, all models are accurately reproduced in the transposed case, where the number of hidden units is smaller than the number of visible ones. On the contrary, about a 20% of the models show large deviations from the exact result when the original, non-transposed dataset is evaluated. This behavior is similarly observed when performing similar calculations with the other datasets with large differences in the number of hidden and visible units.

VI. APPROACHING THE OPTIMAL MEAN FIELD

Despite the simplicity of the expressions in Eqs. (25) and (26), the problem of finding the optimal \mathbf{B}^* can actually be as hard as finding $\log(Z)$ itself, so one has to devise alternative strategies to approximate it.

Three common strategies are usually employed to face this problem. The simplest one is to disregard Eqs. (25) and (26), set $\mathbf{B} = 0$ and sample from the uniform probability distribution, as discussed above. Another common strategy is to set $\mathbf{B} = \mathbf{b}$ from Eq. (13) and to disregard the contributions of the hidden units. Despite its simplicity, the resulting $p_0(\mathbf{x})$ is usually far away from $p_n(\mathbf{x})$. The third approach was devised in [13] for RBM learning, where $\langle \mathbf{x} \rangle_n$ is approximated by its average over the training set. However, this procedure can not be employed when a training set is lacking, as when dealing with magnetic spin systems for instance, or when the existing training set does not properly represent the underlying probability distribution of the system.

In this work we introduce two alternative strategies to estimate \mathbf{B}^* that, on the one hand, imply a low computational cost, and on the other, avoid some of the drawbacks of the aforementioned choices. They both rely on finding a suitable approximation to compute $\langle \mathbf{x} \rangle_n$ in Eqs. (25) and (26). At this point many different choices are possible, while keeping in mind that none of them will perfectly reproduce the exact $\langle \mathbf{x} \rangle_n$ as we assume the original $p_n(\mathbf{x})$ is intractable. However, one must keep in mind that the resulting probability distribution obtained from them is used as the initial point for AIS, which will afterwards correct that to produce reliable samples of $p_n(\mathbf{x})$.

Among the many possible choices, we introduce the following ones:

- Pseudoinverse (Pinv) approximation: one can look for a state of the complete (visible and hidden) space with large probability. In this case one works directly with the energy, setting to zero the gradients with respect to \mathbf{x} of the expression in Eq. (13). One then finds

$$\mathbf{x}_p = -(\mathbf{W}^+)^T \mathbf{c} \quad (28)$$

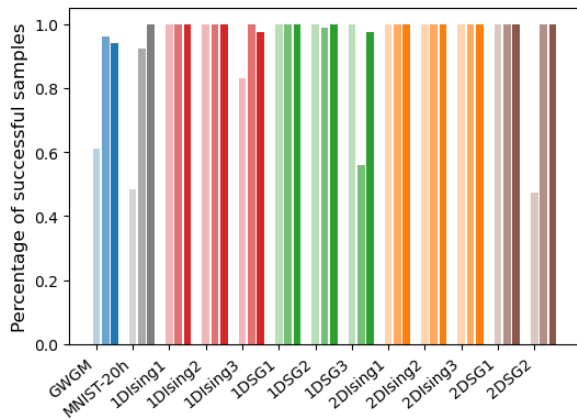


FIG. 5: Percentage of AIS samples with a relative error lower than 0.05% with respect to the exact $\log(Z)$ for the different datasets analyzed. The left, middle and right bars with different gray levels correspond to the predictions starting from $\mathbf{B} = 0$, $\mathbf{B} = \mathbf{B}_{\text{Pinv}}$ and $\mathbf{B} = \mathbf{B}_{\text{Signs}_h}$, respectively.

where \mathbf{W}^+ is the pseudoinverse of the \mathbf{W} matrix. In this work we build \mathbf{x}_p by rounding the result of Eq. (??) to the $[0, 1]$ or the $[-1, 1]$ range, depending on the units used, and approximate $\langle \mathbf{x} \rangle_n$ by \mathbf{x}_p . With that we build the corresponding mean-field bias \mathbf{B}_{Pinv} .

- Signs from Random Hidden (Signs.h): The expectation values $\langle \mathbf{x} \rangle_n$ given in Eq. (27) can only be evaluated when the number of hidden units is small, but unfortunately that is not usually the case in real problems. For that reason we resort to a heuristic approximation, where a set of hidden states $\mathbf{h}^{(\alpha)}$ randomly selected from the uniform probability distribution is used to get the same number of visible states $\mathbf{x}^{(\alpha)}$ from the conditional probabilities $p(x_i^{(\alpha)} = 1 | \mathbf{h}_\alpha) = 1 / (1 + e^{-(b_i + \mathbf{W}^i \mathbf{h}^{(\alpha)})})$. This expression assigns a probability larger than 0.5 to $x_i^{(\alpha)} = 1$ depending on the sign of the argument in the exponential. Following this, we set the components of $\mathbf{x}^{(\alpha)}$ to be equal to 1 when $b_i + \mathbf{W}^i \mathbf{h}^{(\alpha)} > 0$, and to 0 in the opposite case. As in most of the calculations performed in this work, we build a set of 1024 uniformly sampled $\mathbf{h}^{(\alpha)}$ that are used to generate the $\mathbf{x}^{(\alpha)}$ that are finally averaged to get the estimation of $\langle \mathbf{x} \rangle_n$ required to compute the approximated bias $\mathbf{B}_{\text{Signs}_h}$. Notice that this is cost-effective procedure that involves less operations than the pseudoinverse procedure outlined above. This approach is trivially extended to $[-1, 1]$ units.

These two strategies have been used to produce the mean-field probability distributions of Eq. (20) that are used to start AIS. We perform 10 repetitions of each ex-

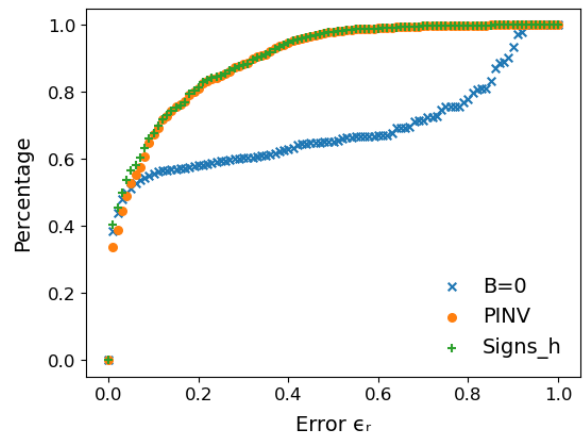


FIG. 6: Percentage of AIS samples with a relative error lower or equal to ϵ_r with respect to the exact $\log(Z)$ for the GWGM dataset.

periment for each model, producing a total of 1000 final values for the GWGM dataset. Figure 5 shows the statistics obtained for all the datasets, corresponding to the total amount of AIS predictions producing a relative error of less than 5% with respect to the exact value of $\log(Z)$. The lighter, midtone and darker bars correspond to $\mathbf{B} = 0$, $\mathbf{B} = \mathbf{B}_{\text{Pinv}}$ and $\mathbf{B} = \mathbf{B}_{\text{Signs}_h}$, respectively. As it can be seen, both Pinv and Signs.h outperforms $\mathbf{B} = 0$ in most cases, yielding similar results in general. It is also worth noticing that for the datasets that do not have bias ($\mathbf{b} = \mathbf{c} = 0$ in Eq.(13)), $\mathbf{B} = 0$ is the optimal \mathbf{B}^* when $[-1, 1]$ units are employed. In this case all three strategies yield very good and similar results.

The fact that both $\mathbf{B}_{\text{Signs}_h}$ and \mathbf{B}_{Pinv} lead to overall better AIS predictions than $\mathbf{B} = 0$ is a direct consequence of the distribution of AIS samples in each case. This is illustrated in Fig. 6 for the GWGM dataset, where all samples generated from all repetitions of all models have been used to account for a better statistics. The plot shows the percentage of samples that have a relative error with respect to the exact $\log(Z)$ equal or lower than ϵ_r , as a function of ϵ_r , for the $\mathbf{B} = 0$, $\mathbf{B} = \mathbf{B}_{\text{Signs}_h}$ and $\mathbf{B} = \mathbf{B}_{\text{Pinv}}$ strategies. As it can be seen, the $\mathbf{B} = 0$ mean field performs worse than the other two in general, although all three strategies produce similar results up to $\epsilon \approx 0.05$. For higher values, though, differences are significant, converging once again towards the end of the curve where all samples fulfill the condition. In any case, we find that $\mathbf{B} = \mathbf{B}_{\text{Signs}_h}$ and $\mathbf{B} = \mathbf{B}_{\text{Pinv}}$ perform very similarly, with minor variations that in the end lead to the small prediction differences displayed in Fig. 5. One can thus conclude that, overall, the samples generated by $\mathbf{B} = \mathbf{B}_{\text{Signs}_h}$ and $\mathbf{B} = \mathbf{B}_{\text{Pinv}}$ are closer to the exact value of $\log(Z)$ than the set produced by $\mathbf{B} = 0$. Despite that, one could argue that in all cases there is always a large amount of samples that fail to

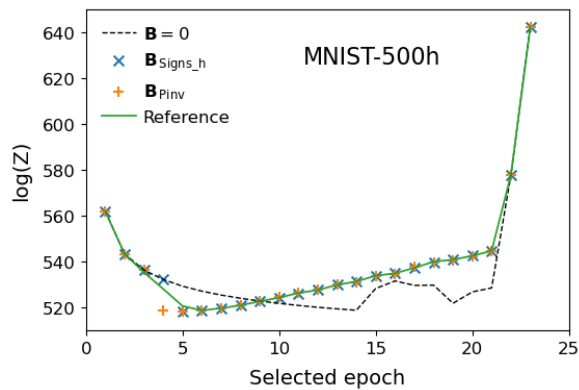


FIG. 7: Comparison of the AIS estimation of $\log(Z)$ along learning for the MNIST dataset with 500 hidden units obtained starting from the different mean field probability distributions discussed in this work. The first points correspond to the first learning epochs, while the last ones show the predictions obtained at an intermediate learning stage.

predict anything close to the right value. However, it is worth noticing that this should be the case due to the stochastic nature of the AIS algorithm and the exponential way in which the generated samples have to be combined, as displayed in Eq. (12). Fluctuations above the exact value of $\log(Z)$ are exponentially amplified, and have to be compensated by a large amount of samples that underestimate its value, whose contribution is exponentially diminished. We can thus conclude that the AIS algorithm has to produce a lot of apparently bad samples in order to produce an accurate result. Furthermore, this asymmetric generation of samples above and below the exact value leads, when not properly balanced, to an underestimation of $\log(Z)$, as noticed in [27]. This picture, though, can be alleviated by increasing the number of intermediate chains N_β , at the expense of linearly increasing the computational cost.

We finally close the discussion by showing in Fig. 7 the value of the partition function estimated with AIS for the MNIST dataset, using a RBM model containing $N_h = 500$ hidden units. For this system, due to its large size, there is no exact calculation of $\log(Z)$ and one has to rely on the predictions obtained employing state-of-the-art techniques found in the literature. For that matter we take as reference the value obtained from the procedure outlined in Ref. [13], where the dataset used to train the RBM is also employed to approximate the mean values required for the evaluation of \mathbf{B}^* in Eqs. (25) and (26). With this, we run AIS with $N_s = 1024$ and $N_\beta = 2^{20}$ to obtain the reference value (green solid line in the figure). Notice that N_β is unreasonably large compared to what one would normally use in order to obtain an as accurate as possible approximation of $\log(Z)$ with the same number of samples used along this work. The figure shows

also the estimations obtained using $\mathbf{B} = 0$, $\mathbf{B} = \mathbf{B}_{\text{Signs}_h}$ and $\mathbf{B} = \mathbf{B}_{\text{PInv}}$ (dotted line, crosses and plus symbols, respectively). The first 21 points correspond to the first 21 learning epochs where the RBM weights rapidly evolve, while the last two points correspond to epochs 40 and 100. As it can be seen, all curves merge at the highest epochs, while the $\mathbf{B} = 0$ prediction departs from the reference curve at the early and intermediate epochs. On the contrary, the selected strategies are hardly distinguishable from the reference line along the whole curve. Despite the differences between the $\mathbf{B} = 0$ curve and the rest are small, one should realize that the computational cost involved in using the proposed strategies is very low, while the prediction obtained are closer to the reference value. This is something that should be taken into account if the goal is to get the most accurate but economic prediction of $\log(Z)$.

VII. SUMMARY AND CONCLUSIONS

To summarize, we have analyzed the performance of the AIS algorithm in the evaluation of the partition function Z of a Restricted Boltzmann Machine with a reduced number of samples and intermediate chains. We evaluate $\log(Z)$ for a number of exactly solvable models which contain a reduced number of hidden units, as well as in standard physical magnetic spin problems where the exact value of $\log(Z)$ is also known. In particular we show that a suitable starting probability distribution $p_0(\mathbf{x})$ of the mean field form can lead to a big improvement of the AIS estimation of $\log(Z)$ for fixed number of samples and intermediate chains. In this scheme, we build $p_0(\mathbf{x})$ from a RBM with bias terms only corresponding to a local external magnetic field, and show that the optimal mean field that minimizes the Kullback-Leibler distance to the RBM probability distribution is directly related to the averages of the visible states. Remarkably, our methodology does not require a training set, and thus it can be used when none is available. The procedure requires only sampling the RBM.

We also propose two simple strategies to approximate the optimal mean field for large systems where the exact averages can not be computed. These result from a trade-off between simplicity, reduced computational cost, and accuracy. The first strategy requires the pseudo-inversion of the matrix of weights, while the second is much cheaper and involves only checking the signs of a linear transformation of it. Overall, both strategies perform equal or better than the standard procedure that starts from $\mathbf{B} = 0$ in the datasets analyzed where $\log(Z)$ is directly accessible. Finally, we also test them on the MNIST dataset with 500 hidden units, to show that the estimations obtained are in excellent agreement with the ones from the procedure outlined in Ref. [13]. We expect that the strategies proposed can be used as the starting point in further studies of $\log(Z)$ in RBMs with the AIS algorithm, either in isolated form or combined.

Acknowledgments

AP and JM acknowledges financial support from grant reference PID2021-124297NB-C32 funded by MICIU/AEI/10.13039/501100011033 and by the *European Union NextGenerationEU/PRTR*. FM and JM. thank the Generalitat de Catalunya for the grant *Grup de Recerca SGR-Cat2021 Condensed, Complex and Quantum*

Matter Group reference 2021SGR-01411. FM: This work has been supported by the Ministerio de Ciencia e Innovación MCIN/AEI/10.13039/501100011033 (Spain) under Grant No. PID2020-113565GB-C21. ER: This work was partially supported by MINECO project PID2022-143299OB-I00 (Spain). Part of the hardware used for this research was donated by the NVIDIA[®] Corporation.

-
- [1] H. B. Callen, *Thermodynamics and an introduction to thermostatistics*, Wiley, New York, (1985).
- [2] R. K. Pathria, *Statistical Mechanics*, Elsevier, (2016)
- [3] K. Huang, *Statistical mechanics*, John Wiley & Sons, (1987).
- [4] L. A. Goldberg, and M. Jerrum, PNAS **112**, 43, 13161–13166, (2025).
- [5] P. Smolensky, *Parallel Distributed Processing: Explorations in the Microstructure of Cognition* vol. 1, edited by D. E. Rumelhart and J. L. McClelland, MIT Press, (1986).
- [6] Y. Bengio, *Learning deep architectures for AI*, Foundations and trends in Machine Learning **2**, 1, 1-127, (2009).
- [7] C. H. Bennett, *Efficient estimation of free energy differences from Monte Carlo data*, J. Comp. Phys, 22(2), 245-268, (1976).
- [8] D. P. Landau, Shan-Ho Tsai, and M. Exle, *A new approach to Monte Carlo simulations in statistical physics: Wang-Landau sampling*, Am. J. Phys. **72**10, (2004).
- [9] C. Zhou, T. C. Schulthess, S. Torbrügge, and D. P. Landau, *Wang-Landau Algorithm for Continuous Models and Joint Density of States*, Phys. Rev. Lett. **96**, 120201 (2006).
- [10] T. Vogel, Y. W. Li, T. Wüst, and D. P. Landau, *Generic, Hierarchical Framework for Massively Parallel Wang-Landau Sampling*, Phys. Rev. Lett. **110**, 210603 (2013).
- [11] R. M. Neal, *Annealed Importance Sampling*, Statistics and Computing **11**, 125–139, (2001).
- [12] R. M. Neal, *Annealed Importance Sampling*, technical Report 9805, Dept. Statistics, University of Toronto, (1998).
- [13] R. Salakhutdinov and I. Murray, *International Conference on Machine Learning* 872-879, (2008).
- [14] D. M. Ceperley, Rev. Mod. Phys. **67**, 279, (1996).
- [15] I. Kosztin, B. Faber, and K. Schulten, Am. J. Phys. **64**, 633 (1996).
- [16] A. Sarsa, K. E. Schmidt, and W. R. Magro, J. Chem. Phys. **113**, 1366 (2000).
- [17] R. Srinivasan, *Importance sampling: Applications in Communications and Detection*, Springer Verlag, (2002).
- [18] D. J. Amit, *Modelling Brain Function: The World of Attractor Neural Networks*, (Cambridge University Press, New York, NY, USA, 1989), 1st ed., ISBN 0521361001.
- [19] G. E. Hinton, and R. R. Salakhutdinov, Science **313**, 504 (2006).
- [20] R. R. Salakhutdinov, A. Mnih, and G. E. Hinton, in *Proceedings of the 24th international conference on Machine learning*, (ACM, 2007) pp. 791–798.
- [21] S. Geman, and D. Geman, IEEE Transactions on Pattern Analysis and Machine Intelligence **6**, 721 (1984).
- [22] P. M. Long, and R. A. Servedio, *International Conference on Machine Learning*, 703-710, (2010).
- [23] <http://yann.lecun.com/exdb/mnist>
- [24] E. Ising, Z. Phys, 31(1), 253-258, (1925).
- [25] J. J. Binney, N. J. Dowrick, A. J. Fisher, and M. E. J. Newman, *The theory of critical phenomena: an introduction to the renormalization group*, Oxford University Press, (1992),
- [26] L. Onsager, Phys. Rev. **65**, 3 and 4, 117, (1944).
- [27] Y. Burda, R. Grosse, and R. Salakhutdinov, *Accurate and conservative estimates of MRF log-likelihood using reverse annealing*, in *Artificial Intelligence and Statistics*, 102–110, PMLR, 2015.